National Institutes of Justice, Forensics R&D

AWARD NUMBER: 2018-R2-CX-0033

FINAL RESEARCH REPORT

PROJECT TITLE: "Physical Characteristics of Spatter Stains on Textiles: Influence of Impact Surface Texture, Blood Drop Volume and Blood Drop Velocity"

PI: Tiegang Fang, Professor, Department of Mechanical and Aerospace Engineering, North Carolina State University
Address: 3246 Engineering Building III, 1840 Entrepreneur Drive - Campus Box 7910, Raleigh, NC 27695-7910
Telephone: (919) 515-5230
Email: tfang2@ncsu.edu

Submitted by: Stefanie Saunders, Associate Director, Operations, Office of Sponsored Programs
Email: sps@ncsu.edu
Telephone: (919)515-2444

Recipient Organization: North Carolina State University
Address: Administrative Services III Suite 240, 2601 Wolf Village Way, Campus Box 7514, Raleigh, NC 27695-7514

Recipient DUNS and EIN:

Project Period: January 1, 2019 – June 30, 2021

Award Amount: $272,463

Stefanie D. Saunders

Authorized Signature

Stefanie D. Saunders, Associate Director, Ops. - Sponsored Programs

Digitally signed by Stefanie D. Saunders, Associate Director, Ops. - Sponsored Programs
Date: 2021.09.07 15:07:00 -04'00'

Date

PROJECT SUMMARY

Although bloodstain pattern analysis (BPA) has become a well-established forensic science, the 2015 operational requirements published by the National Institutes of Justice state that "Fundamental understanding of blood properties, droplet formation, droplet flight and the resultant formation of bloodstain patterns" demands a better foundation. Validated BPA models are lacking as indicated by a previous NIJ report, in which more than 12% error rates were reported for BPA on rigid surfaces and even higher rates on textiles [1]. Regarding the formation of bloodstain patterns on textiles, although blood drop generation events are identical, many uncertainties in the interpretation could be involved due to the complex alteration by the textiles, *i.e.*, absorption of blood drop kinetic energy by deflection or deformation of the textile, partial penetration of blood drop through the textile grid, enlargement of bloodstain by the subsequent wicking within the textile yarns, *etc*. [2-3]. As revealed by Ref. [4], the impacting process of a blood drop on a fabric surface and its subsequent wicking process are distinct in affecting the final bloodstains. Therefore, there is a necessity of investigation into the fundamental blood drop dynamics during impact and subsequent wicking in the process of bloodstain formation on textiles.

MAJOR GOALS

The goal of the project is to gain a detailed, fundamental understanding of the physics and dynamics of airborne blood as it impacts textile surfaces during the creation of bloodstains, particularly for blood droplets with diameters ranging from a few hundred microns up to four millimeters that represent the case of impact spatter formation. Specifically, the project focused on the influence of the textile surface texture, blood drop volume, and blood drop velocity on ***a*** the dynamics of single blood droplet impacting complex textile surfaces and ***b*** the resultant bloodstain patterns. Thus, the project goal was accomplished by the following specific tasks:

1) Creation and characterization of target textile surfaces with complex structure.
2) Investigation and analysis of blood droplet impact dynamics on textile surfaces.

3) Investigation and analysis of blood droplet wicking dynamics and the resultant bloodstains on textile surfaces.

To enable the research into single micro-sized blood droplet interaction with textile surface for micro-sized spatter formation on textiles, a secondary goal was to create and evaluate a single micro blood droplet generation system for forensic science research which can reliably generate micro-sized blood droplets with controlled diameter and velocity.

RESEARCH QUESTIONS

The research question to be resolved in this project was to determine what roles the blood drop velocity, drop volume and target surface texture play in the formation of spatter stains on textile substrates, for practitioners in the field of BPA.

RESEARCH DESIGN AND METHODS

This study was designed to provide important scientific foundations that are fundamental in improving the bloodstain pattern analysis technique for interpreting spatter bloodstains on textiles. An overview of the approach design is demonstrated in Fig. 1, which briefly describes the materials, experiment design, measurement setup, data analysis, and potential impact generated from this research. The implementation of this approach enabled us to reveal the underlying physics in the bloodstain formation process, in terms of blood drop impact dynamics and blood drop wicking dynamics, through the customized imaging setup. In-depth examination of the resultant bloodstains helped evaluate the influence of the blood drop impact and wicking dynamics on the final bloodstain formation. A variety of experimental conditions were designed to investigate the effects of drop impact velocity, types of fabrics, and surface inclination angles on the bloodstain formation. Micro-sized blood droplet experiments were conducted to evaluate the micro blood droplet generation and to represent the micro-sized blood spatter stain formation. The details of materials and measurement setup utilized in this project are summarized in the following subsections.

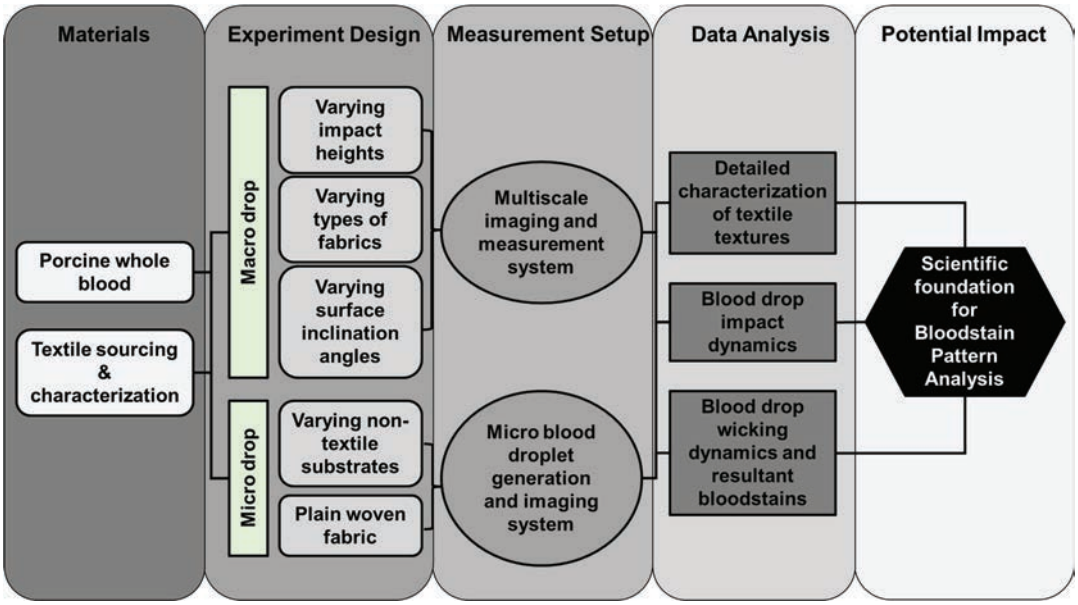

Figure 1. Overall research design. Overview of the approach design, including the materials, experiment design, measurement setup, data analysis, and potential impact generated in this project.

1) Porcine whole blood

Anticoagulated K2-EDTA added) porcine whole blood purchased from Innovative Research Inc. was used in this project as a substitute to human blood. The details regarding blood storage and preparation procedure before each set of experiments can be found in our recent publication [5]. Within this project, three individual sets of blood purchase were made. The major physical properties of the blood, as summarized in Fig. 2, were slightly different among different sets of blood, in terms of the density ρ, surface tension σ), and blood dynamic viscosity μ). The details of the measurement methods for ρ, σ, and μ can also be found in Ref. [5]. Generally, the blood shear-thinning behavior was well presented. A power-law fluid model was employed to fit the experimental results, and the asymptotic viscosity at an infinite shear rate η_{inf}) was obtained. η_{inf} was generally used as the characteristic viscosity of the porcine blood when calculating dimensionless numbers, *i.e.*, Reynolds number ($Re = \rho U D_0/\mu$.

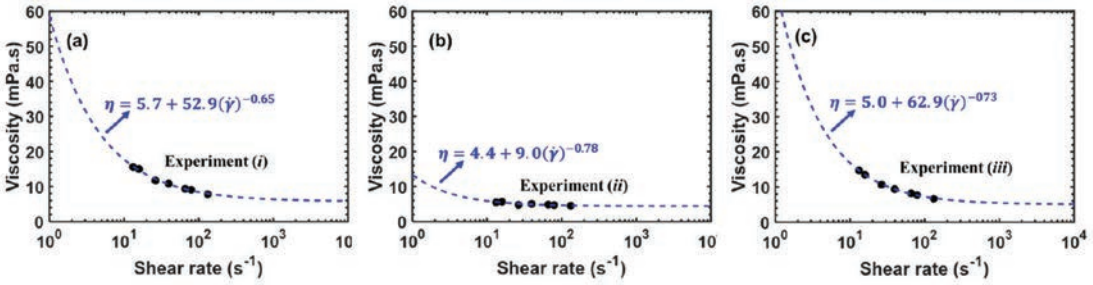

(d)

Experiment	Density (g/mL)	Dynamic Viscosity @ $\dot{\gamma}_\infty$ ($mPa.s$)	Surface Tension (mN/m)
(*i*)	1.04	5.7	60.3
(*ii*)	1.05	4.4	59.9
(*iii*)	1.05	5.0	59.4

Figure 2. Characterization of the porcine whole blood. (a)-(c) Experimental measurement and power-law fluid model fitting of the blood viscosity at different shear rates for different sets of blood purchased at different time. (d) Summary of the primary physical properties of porcine whole blood used in the project.

2) Textile sourcing and characterization

The fabrics investigated in this project were 100% cotton plain woven, 100% cotton 3×1 twill, and 100% cotton jersey knit. Standard laboratory practice for home laundering fabrics by AATCC monograph M7 was carried out on all fabrics to simulate a rigorous home laundering [6] to make the fabrics suitable for experiments. After the fabric laundering process, samples of 10"×6" (25.4cm×15.2cm were cut and ironed to remove wrinkles.

The characterization of these fabrics was carried out at different levels, including the fabric structure, yarn properties, and surface roughness. The 3D fabric structures were reconstructed from a confocal laser scanning microscope Keyence VKx1100) and are demonstrated in Figs. 3(a)-(e) for different types of fabrics. It should be noted that for twill fabric and knit fabric, surface textures of the technical front and technical back are distinct from each other. Therefore, blood drop impact and wicking dynamics and the

This resource was prepared by the author(s) using Federal funds provided by the U.S. Department of Justice. Opinions or points of view expressed are those of the author(s) and do not necessarily reflect the official position or policies of the U.S. Department of Justice.

bloodstains formed at the same blood drop generation condition could be drastically different on the two sides of a twill or knit fabric.

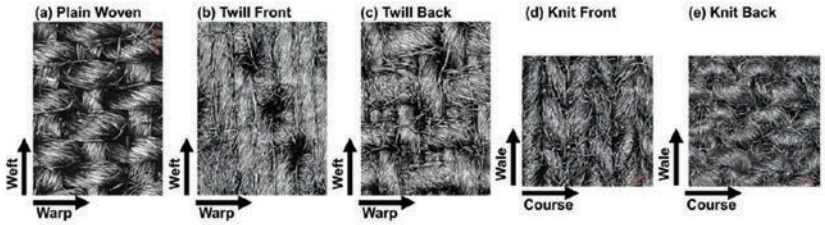

(f)

Fabric	Yarn	Linear density (g/m)	Yarn number		
			Denier [a]	Dtex [b]	Ne [c]
Plain Woven	Warp	0.01427	128	143	41.4
	Weft	0.01413	127	141	41.8
3×1 Twill	Warp	0.02586	232.7	259	22.8
	Weft	0.05393	485.4	539	11.0
Jersey Knit	Wale Course	0.02210	198.9	221	26.7

[a] Denier=g/9000m; [b] Dtex=g/10000m; [c] Ne=5905 Dtex

(g)

Fabric Surface	Surface Roughness, *Sa* (μm)	Line Roughness Parameter					
		Ra (μm)			Rsm (μm)	Rpk (μm)	
Plain Woven	24.1 ± 0.9	Warp	Weft	Warp	Weft	Warp	Weft
		16.5	17.6	232	240	22.0	18.0
Twill Front	35.9 ± 1.5	Warp	Weft	Warp	Weft	Warp	Weft
		35.3	34.4	303	452	39.8	41.6
Twill Back	37.5 ± 3.2	Warp	Weft	Warp	Weft	Warp	Weft
		16.9	33.7	257	419	32.0	39.5
Knit Front	60.4 ± 8.0	Wale	Course	Wale	Course	Wale	Course
		42.2	54.7	299	203	96.2	86.9
Knit Back	70.2 ± 8.4	Wale	Course	Wale	Course	Wale	Course
		53.4	55.8	212	442	71.9	73.6

Figure 3. Characterization of the textile substrates. a)-(e) Confocal images for different fabric structures, (f) yarn properties of each type of fabric, and (g) surface roughness and line roughness for five different fabric structures.

Yarn properties are summarized in Fig. 3(f) for the three types of fabrics. Yarn number and linear density were measured according to the ASTM D1059-17: Standard Test Method for Yarn Number Based on Short-Length Specimens [7]. Warp and weft yarns for the plain woven fabric generally share similar properties in terms of the linear density. On the contrary, for the twill fabric, the weft yarn has a higher linear density than the warp yarn. The difference in the yarn properties plus the woven nature of the fabric make the fabric surface a highly inhomogeneous textured surface which can lead to strong irregularities in

the resultant bloodstains. The roughness measurement was conducted for all the five different fabric structures (Plain Woven, Twill Front, Twill Back, Knit Front, Knit Back) in terms of the area roughness Sa, arithmetical mean height of an area on the fabric). The area roughness was measured within different regions of interest (ROI) on the fabric sample. The results showed that the roughness difference among different ROIs was not statistically significant $F_{calculated}<F_{critical}$. The average surface roughness for the five fabric structures and the line roughness R_a, defined as the arithmetical mean height of a line on the fabric) along warp/weft or wale/course directions were summarized in Fig. 3(g). The confocal microscope workstation top surface was used as the reference plane for the measurements.

3) Multiscale imaging and measurement system

To record a full history of bloodstain formation process, which includes drop impact, drop wicking, and drop drying process, a multiscale imaging system was constructed. Figure 4 demonstrates such an imaging system used in this project, which consists of the high-speed low-speed video recording setup, macroscopic imaging setup, and microscopic bloodstain imaging setup.

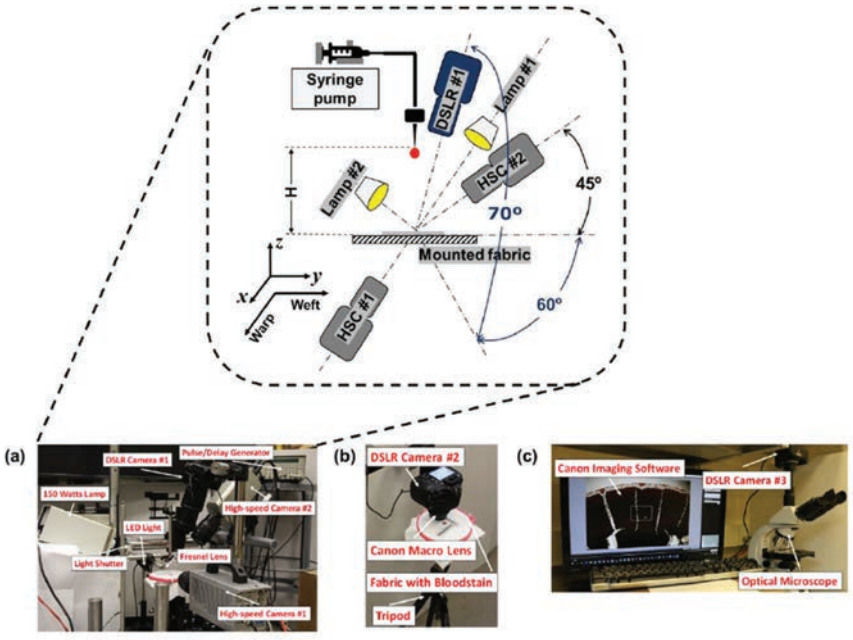

Figure 4. The customized multiscale imaging system including (a) high-speed & low-speed video recording setup, (b macroscopic bloodstain imaging setup, and (c) microscopic bloodstain imaging setup.

4) Micro blood droplet generation and imaging system

To investigate the sub-millimeter blood droplet impacting and bloodstain formation for spatter stains on textiles, a customized piezoelectric micro blood droplet generation system was built as shown in Fig. 5(a). The whole setup consists of three major components, in terms of a customized liquid manipulation system, a customized electronics control for driving the piezoelectric nozzles (MicroFab Technologies, Inc.), and a commercial pneumatic controller (MicroFab Technologies, Inc.).

Figure 5(b) shows the whole experiment setup for conducting micro blood droplet experiments, including the micro droplet generation system and high-speed visualization system. Compared to the previous "multiscale imaging system" which was meant for visualizing macro-sized blood drops, a zoom lens with a much higher magnification (12×) was utilized with a high-speed camera for the visualization of the micro droplet generation process and droplet impact process on the surface, separately. In addition, a high-intensity LED light Nila Zaila Bi-Color, 45W) was used in the experiments to provide sufficient light intensity for backlighting illumination without heating the ambient too much. The trigger of the high-speed video camera and the generation of a single blood droplet were synchronized by a digital delay/pulse generator (Stanford DG535) to ensure capturing the full micro blood drop impacting process.

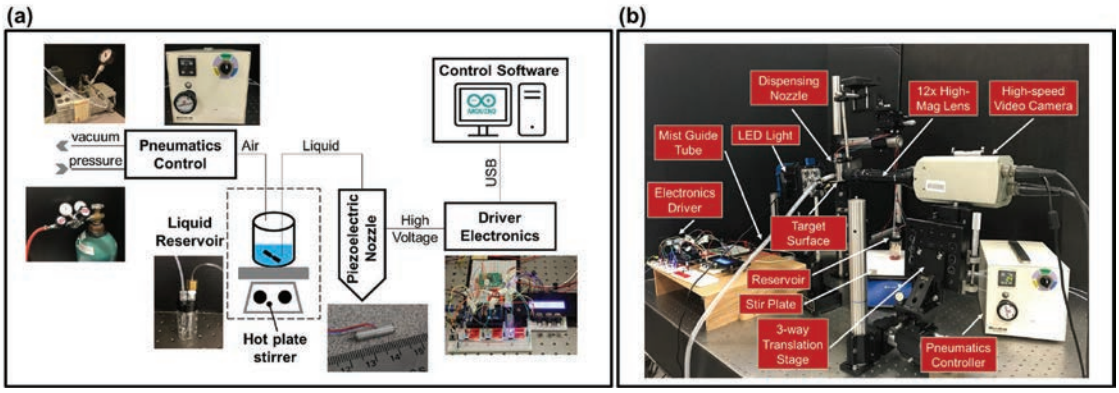

Figure 5. Micro blood droplet generation and imaging system. (a) Overview of the single micro droplet generation system. (b) The experimental setup, including the droplet generation and high-speed visualization system for micro blood droplet generation and impact experiment.

DATA ANALYSIS

The videos showing blood drop impacting and wicking dynamic process, which were captured by the high-speed camera and low-speed DSLR camera, were processed via a customized image processing code in MATLAB. The image processing routine automatically calculated important parameters (blood drop diameter D_0, impact velocity U_0, spreading diameter $D(t)$ or area $A(t)$, *etc.*) for characterizing droplet impact and wicking dynamics for each frame at different time instants in a batch mode.

It is shown from Fig. 4 that the high-speed camera and DSLR camera capturing bloodstain evolution were tilted by a certain angle, therefore presenting certain perspective projection errors in the original image frames. To achieve an accurate measurement of the bloodstain shapes, an Inverse Perspective Mapping (IPM) method as shown in Fig. 6 was employed to reconstruct the bloodstain shapes. The customized IPM algorithm could restore the original distorted bloodstains and made the scaling uniform across the view field as shown in Figs. 6(a)-(b). By using the bloodstain images captured by the macroscopic imaging setup (Fig. 4b, camera lens perpendicular to the fabric surface) as a baseline, it was shown that the IPM algorithm could well restore the distorted bloodstain images from the tilted cameras (Figs. 6c-d).

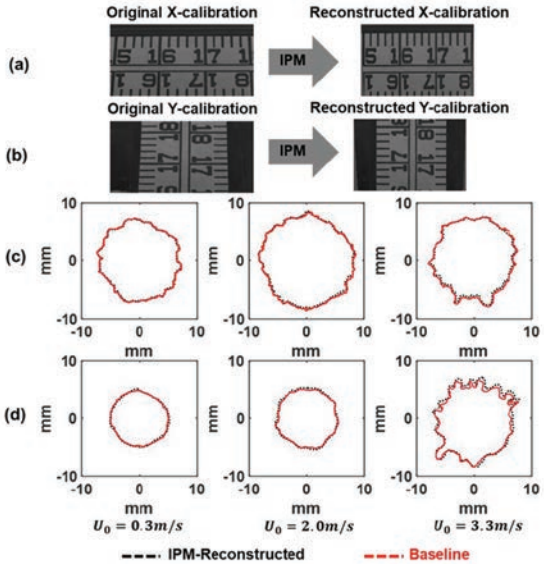

Figure 6. The proposed IPM reconstruction technique. Sample IPM reconstruction of calibration rulers for a tilted high-speed camera demonstrated in (a) X- direction, (b) Y-direction. Validation of the IPM reconstruction for the bloodstain images from c) a DSLR camera and (d) a high-speed camera.

This resource was prepared by the author(s) using Federal funds provided by the U.S. Department of Justice. Opinions or points of view expressed are those of the author(s) and do not necessarily reflect the official position or policies of the U.S. Department of Justice.

EXPECTED APPLICABILITY OF THE RESEARCH

The current implementation of bloodstain pattern analysis (BPA) technique for bloodstains on textiles is still empirical and lacking solid scientific foundation regarding how these bloodstains are formed on these complex textured surfaces. The study carried out in this project provides such fundamental scientific knowledge from the viewpoint of fluid mechanics, particularly regarding how blood drop spreads on the textiles after its impact, how the subsequent wicking alters the bloodstain shape and area before the stain dries out, what key characteristics of the bloodstains can be utilized in BPA to provide more reliable interpretations, how much the uncertainty would be when reconstructing the blood drop size, velocity, and angles of impact based on the bloodstains, *etc.*. Therefore, the outcomes of this project can be used as a reference for practitioners in the BPA field when practicing BPA on textile-type surfaces.

PARTICIPANTS AND OTHER COLLABORATING ORGANIZATIONS

Dr. Stephen Michielsen served as the project PI from January 2019 to August 2019. Dr. Tiegang Fang served as the project PI from September 2019 to June 2021. Dr. Vanessa Gallardo (staff scientist) and Mr. Fujun Wang (graduate student) conducted the experiments, data collection, and data post-processing. Mr. Kaushik Nonavinakere Vinod (graduate student) also contributed to the experiments on micro droplets.

CHANGES IN APPROACH FROM ORIGINAL DESIGN AND REASON FOR CHANGE

There were no changes to the original approach, which tried to address the research question through a systematic, parametric study of the influence of textile types, angles of impact degrees, drop diameter, drop velocity, and textile orientation. There were several design conditions that were not tested compared to the original experimental design in the proposal, which however did not affect much of the interpretation of the current dataset to address the research questions in this project. Specifically,

1) For the parameter of "droplet diameter" *or* drop volume), two conditions one for micro drop, one for macro drop) were investigated instead of the original four design conditions two for micro drop, two for macro drop).
2) For the parameter of "textile type", Terry cloth was not tested.
3) For the parameter of "drop velocity", 10m/s impact velocity was not tested. The highest blood drop impact velocity achieved in the project was around 8m/s.

OUTCOMES

ACTIVITIES/ACCOMPLISHMENTS

The major accomplishments in this project are summarized as follows:

1) A multiscale imaging system was specifically constructed for BPA research in this project, which enabled recording a full history of bloodstain formation on fabrics including both the instantaneous blood drop impact process and the slow but long-time post-impact wicking process in the fabrics.
2) Based on the customized multiscale measurement system, high-speed videos from side view and tilted view showing blood drop impacting process, high-definition videos showing blood drop post-impact wicking process, macroscopic (1× MAG) images showing bloodstains at 5 minutes and 24 hours after impacting, microscopic (10× MAG) images showing bloodstains at 5 minutes and 24 hours after impacting were collected and analyzed to investigate the influence of blood droplet impact velocity, textile surface texture, and surface inclinations.
3) At the completion of this project, comprehensive analysis and theoretical modeling were finished for blood droplet impacting and wicking on plain woven fabric surfaces at different impacting velocities. Corresponding work has been published in *Forensic Science International*.
4) A customized, piezoelectric single blood droplet generation system was constructed and tested. Regime maps of pulse widths for stable blood droplets generation were obtained.

5) High speed videos (15,000 frame/second) showing the super-fast micro blood droplet impact process on three types of solid surfaces (glass, Teflon, and silicon wafer) were obtained and analyzed.

RESULTS AND FINDINGS

Based on the multi-scale imaging system, both the blood droplet impact/wicking dynamics and the resultant bloodstains on fabric surfaces were comprehensively studied in this project. The presentation of the results and findings is organized as follows. The blood drop impact and wicking dynamics on fabric surfaces will first be discussed at the conditions with different impact velocities, different fabrics, and different surface inclinations. After that, the bloodstains formed on the fabric surfaces will be analyzed.

1) Blood drop impact and wicking dynamics – influence of impact velocity

Figure 7(a) demonstrates sample image sequences from different cameras in the "multi-scale imaging" system, which combine to depict the whole temporal evolution of blood droplet morphology after impacting onto the fabric surface, including both the instantaneous impact-induced spreading process and the capillary-induced wicking process. Following the concept of typical time sequence of spreading and wicking for blood drop impacting on fabrics [4], distinct stages were classified based on the spreading curves (bloodstain area *Vs* elapsed time) as shown in Fig. 7(b), which are the *i*) inertial impact regime, *ii* initial absorption regime, *iii*) 1st-stage wicking regime, *iv*) 2nd-stage wicking regime, and *v*) the final equilibrium regime. The most obvious effect of the wicking process in altering the bloodstain is to increase the bloodstain area. Figure 7(c) quantitatively characterizes the maximum spread factor right after impact ($\beta_{i,e} = A_{i,e}/\left(\frac{1}{6}\right)\pi D_0^3$) and the final spread factor ($\beta_{i,f} = A_{i,f}/\left(\frac{1}{6}\right)\pi D_0^3$) at the end of the wicking process. It is shown from Fig. 7(c) that $\beta_{i,e}$ increases significantly with the increase of the Weber number while $\beta_{f,e}$ remains constant for different Weber numbers. The average equivalent final stain factor was found to be $\bar{\beta}_{f,e} = 4.53$. This specific value should be related to the original blood drop volume and the fabric porosity characteristics; and it could be estimated based on the previous theories developed in Refs. [8-9].

In addition to enlarging the bloodstain area, the wicking process makes the bloodstains on textiles highly distorted *e.g.*, the image frame at 50s in Fig. 7a), compared to bloodstains formed on rigid, non-porous surfaces. After a blood droplet impacts on the fabric surface, the initial absorption would usually

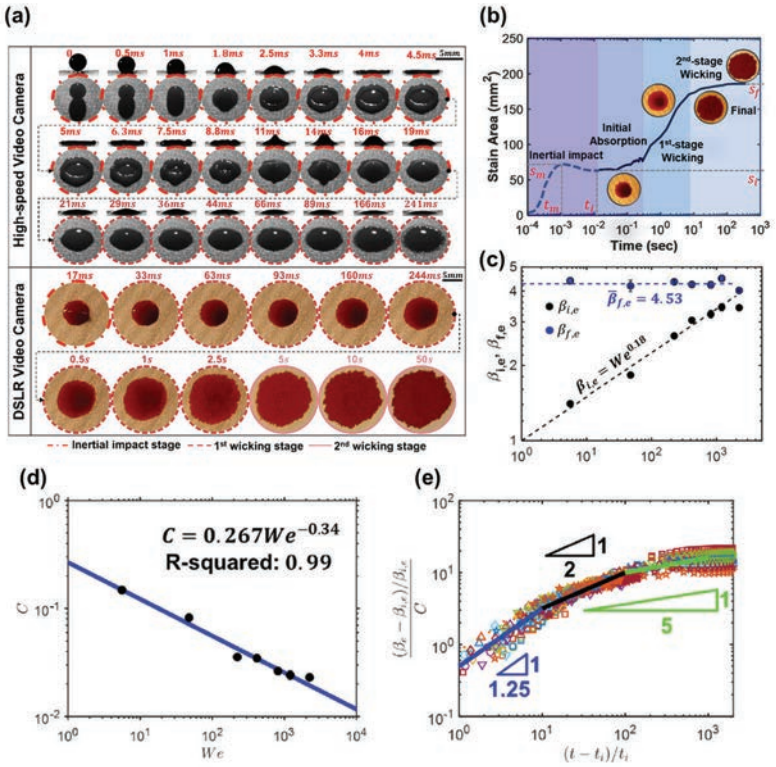

Figure 7. Blood droplet impact and wicking dynamics at different impact velocities. (a) Blood droplet morphology during its impact and wicking process on plain woven fabric surface; (b) A detailed regime classification for blood droplet post-impact process on the plain woven fabric surface; (c) The variation of the impact-induced maximum spread factor ($\beta_{i,e}$) and the final spread factor ($\beta_{f,e}$) for blood drop impacting onto plain woven fabric surfaces at different Weber numbers; (d) The wicking coefficient C at different Weber numbers; (e) Collapse of all the curves in the "first-wicking regime".

occur before the wicking process. During the initial absorption, the blood is mainly drawn vertically to fill up the capillary channels. When the yarns below the impact-induced area become saturated, the radial wicking process starts; and the bloodstain area increases dramatically during the first-wicking stage as shown in Fig. 7(b). Such a wicking process typically lasts for a few seconds and after that, the much longer and slower second wicking stage will dominate. As has already been discussed, the first wicking stage mainly contributes to the increase of the bloodstain area while the second wicking stage mainly affects the

This resource was prepared by the author(s) using Federal funds provided by the U.S. Department of Justice. Opinions or points of view expressed are those of the author(s) and do not necessarily reflect the official position or policies of the U.S. Department of Justice.

irregularities on the edge of those bloodstains. More than that, it is shown in Fig. 7(b) that these two wicking stages feature different slopes.

The Washburn equation [10] is usually used to depict the wicking (or imbibition) of liquid from an infinite reservoir in 1-D case [11]. For wicking from a finite reservoir, an equation $A = K(\gamma/\eta)^u V_0^m t^n$ is developed [12]. In the equation, A is the wicking area, K is the fabric sorption coefficient, and V_0 is the droplet volume. Such a correlation cannot be used in the current study, as the initial area before the wicking occurs cannot be neglected, which is a basis for deriving the equation above. Instead, a different semi-empirical correlation was proposed for describing the blood droplet post-impact wicking dynamics during the first-stage wicking regime as follows:

$$\frac{e-\beta_{i,e}}{i,e} = C\left(\frac{t-t_i}{t_i}\right)^{1/2}. \quad (1)$$

The detailed derivation of this semi-empirical correlation was documented in Ref. [5]. In the above equation, C is defined as the "wicking coefficient". By fitting the experimental data to the Eq. (1), the wicking coefficients at different impact velocities *i.e.*, different Weber numbers) were determined as demonstrated in Fig. 7(d). It is shown that the variation of the wicking coefficient can be well predicted by a power law correlation with respect to the impact Weber number: $C \sim 0.267We^{-0.34}$. Moreover, after arranging the wicking coefficient to the left of the Eq. (1) and replotting the curves in the log-log scale, it is found that all the spreading curves collapse together as shown in Fig. 7(e). This indicates that a universal governing wicking dynamics exists for the finite blood droplet post-impact wicking process on the plain woven cotton fabric. A detailed examination of the collapsed curves in Fig. 7(e) shows that at the very early stage $(t - t_i)/t_i < 10$), the slope of the collapsed curves is around 0.8. However, after this short period, the slope of the collapsed curves remains 0.5 for a long time until the end of the first-stage wicking process $(t - t_i)/t_i \sim 100$). Therefore, it implies that the Washburn equation (the square root law) for infinite reservoir wicking still applies to the majority of the first-stage wicking process of a finite, impacting blood droplet on plain-woven cotton fabric. When $(t - t_i)/t_i > 100$, the second-stage wicking process starts,

and the slope of the curves decreases to a value close to 0.2, which has been attributed to the influence of drop evaporation [5].

2) Blood drop impact and wicking dynamics – influence of fabric type

In the above subsection, the blood droplet impact and wicking dynamics have been comprehensively discussed at different impact velocities *or* different We) on plain woven fabric surfaces. In this section, the blood drop impact and wicking process on five different fabric surfaces would be analyzed to demonstrate the influence of fabric types.

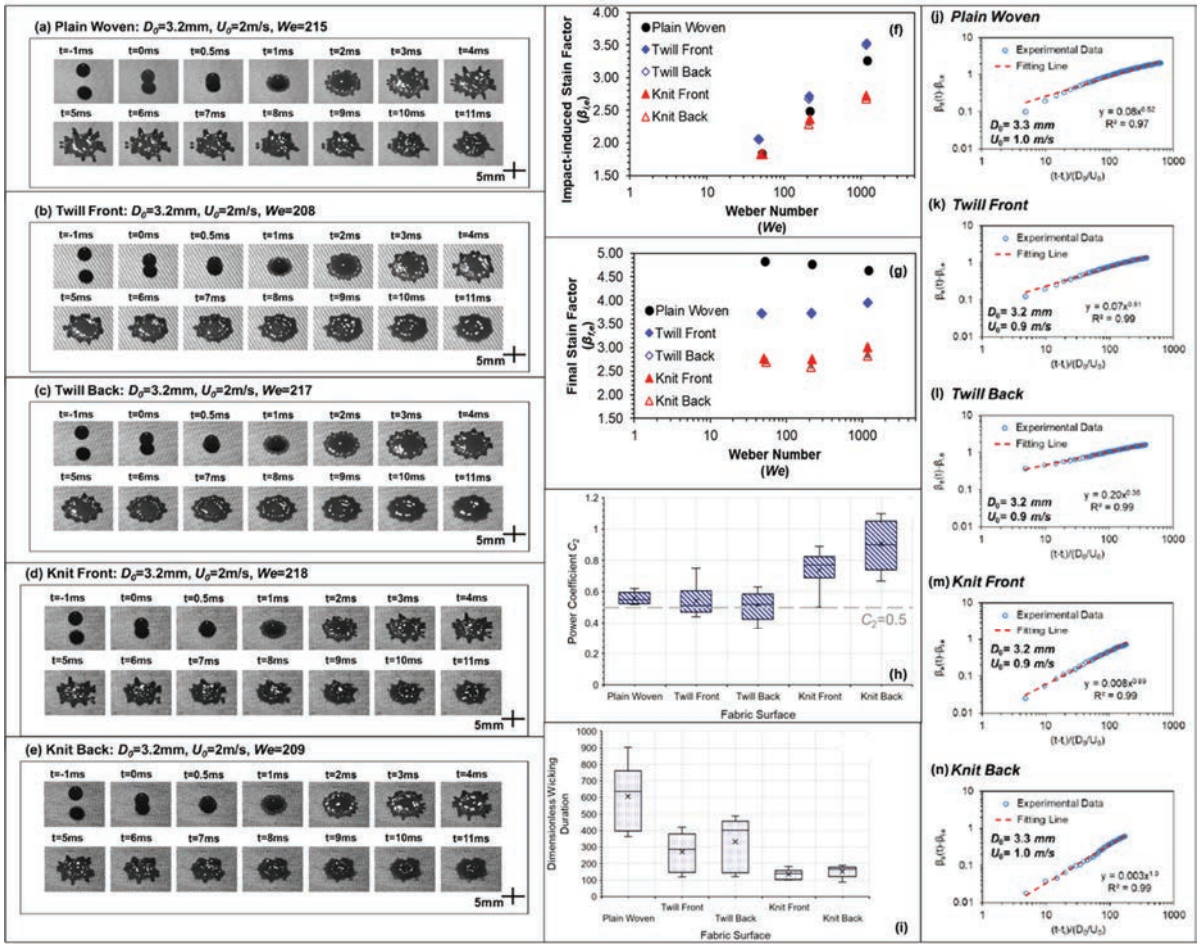

Figure 8. Blood droplet impact and wicking dynamics on different types of fabrics. (a)-(e) Blood droplet impact morphologies at We~210 on plain woven, twill front, twill back, knit front, and knit back fabric surfaces. (f)-(g) Variation of the impact-induced maximum spread factor and the final stain factor at different Weber numbers for different fabric surfaces. (h)-(i Variation of the power coefficient C_2 and the dimensionless wicking duration on the five different fabric surfaces. (j)-(n) Fitting of the semi-empirical correlation to the experimental data for a blood drop impact velocity of $1m/s$ on the five different fabric surfaces.

First, Figures 8(a)-(e) compare the blood droplet impact morphologies at an impact velocity of $2m/s$ on five different fabric surfaces, including the plain woven, twill front, twill back, knit front, and knit back surfaces. For plain woven fabric, the technical front and back are identical. While for the twill and knit fabric, the front and back have different surface textures and different surface roughness (Fig. 3). Therefore, in this project, five types of textile surfaces with distinct textures have been examined. It is shown from Figs. 8(a)-(e) that blood drops impacting on twill fabric (both front and back) experience fewer instabilities than on plain woven and knit fabrics (both front and back): elongated fingers (spines) were observed on the plain woven, knit front, and knit back surfaces, while on twill front and twill back surfaces, the rim of the blood drops only presents some scallops, which are short, rounded convex structures.

As shown in the previous subsection, there are two important stain factors that characterize the bloodstain formations: the impact-induced stain factor ($\beta_{i,e}$) and the final stain factor ($\beta_{f,e}$). Therefore, Figures 8(f) and 8(g) demonstrate the variation of these two characteristic stain factors on the five different fabric surfaces, respectively. It is shown from Fig. 8(f) that $\beta_{i,e}$ on different textile surfaces all increase with the increase of blood drop impact energy (or Weber number). But $\beta_{i,e}$ is the largest on the twill fabric, smallest on the jersey knit fabric, and in-between on the plain woven fabric. It should be noted here that twill fabric has higher surface roughness (Sa) than the plain woven fabric but has larger impact-induced stain factor. This implies that the Sa alone cannot be used to explain the difference in the impact-induced stain factor ($\beta_{i,e}$). Moreover, differences between the two sides of the same fabric are much smaller than differences among different fabric types. In contrast, it is shown from Fig. 8(g) that the final stain factor $\beta_{f,e}$ is more dependent on the fabric types rather than on the impact velocities: minor changes were observed in $\beta_{f,e}$ on plain woven (-4%), twill front (+6%), twill back (+6%), knit front (+8%), and knit back (+8%) surfaces when Weber number increases from ~50 to ~1200. Considering the small variation (<8%) and uncertainties of measurement, the average equivalent stain factor could be used to approximate the equivalent final stain factor for blood drop impacting on plain woven fabric, 3×1 twill fabric, and jersey knit fabric. These average equivalent stain factors ($\bar{\beta}_{f,e}$), for a blood drop with a volume of 17.5μL or a

diameter of $3.2mm$, are 4.75 for plain woven, 3.81 for twill front, 3.79 for twill back, 2.85 for knit front, and 2.71 for knit back.

It has been shown that Eq.(1) can well depict the blood drop wicking dynamics on plain woven fabric surfaces. Because the structures of the twill fabric and knit fabric are not isotropic, Eq. (1) may not be directly employed to fit the corresponding experimental data. Instead, a fitting function with two fitting parameters but still adopting the form of Eq. 1) is proposed as follows when analyzing the first-stage wicking dynamics on different fabric surfaces:

$$\beta_e(t) - \beta_{i,e} = C_1(t^* - t_i^*)^{C_2}. \quad (2$$

C_1 in the above equation is the wicking coefficient as defined in the previous subsection, and C_2 is the power coefficient which characterizes the wicking rate of the blood drop on the fabric surfaces. The focus of wicking dynamics analysis on different fabric surfaces includes the comparison of the power coefficient (denoted by C_2 (Fig. 8h) and the wicking duration Fig. 8i). To obtain these two important wicking parameters, Eq. (2) was fitted to the experimental data for the five fabric surfaces. As shown in Fig. 8(j)-(n), the R-squared values are generally above 0.9, indicating the appropriateness of using Eq. (2) as a general correlation to describe the blood drop wicking process on various types of fabric surfaces.

Back to Fig. 8(h) which plots the wicking power coefficients for different fabric surface, it is shown that the theoretical value of 0.5 can generally approximate the first-stage wicking rate on the plain woven, twill front, and twill back surfaces. No significant difference in C_2 was observed among these three fabric surfaces. In contrast, the values of C_2 are significantly larger on the knit front and knit back surfaces. Moreover, the difference in C_2 between the knit front and knit back surfaces is also relatively more significant than that between twill front and twill back surfaces. On the other hand, as shown in Fig. 8(i), the difference in the dimensionless wicking duration is also significant among different fabric surfaces. Plain woven fabric surface has the longest wicking duration among the five fabric surfaces and single jersey knit fabric has the shortest wicking duration. The wicking duration on the twill fabric surfaces is in-between.

Lastly, according to Fig. 8(i), there is no significant difference in the dimensionless wicking duration between the front and back for the same type of fabric.

3) Blood drop impact and wicking dynamics – influence of surface inclination

In this subsection, the influence of surface inclination *or* droplet impact angle, α) on the blood droplet impact and wicking process was demonstrated on the technical front surface of the twill fabric. Figures 9(a)-(d) summarize typical image sequences from both the side view and the inclined view, which shows blood droplets impacting and wicking on the technical front surface of the twill fabric with different impact angles. $\alpha = 90°$ as shown in Fig. 9(a) is used as a control, of which the spreading and wicking characteristics have been extensively described in the previous subsections.

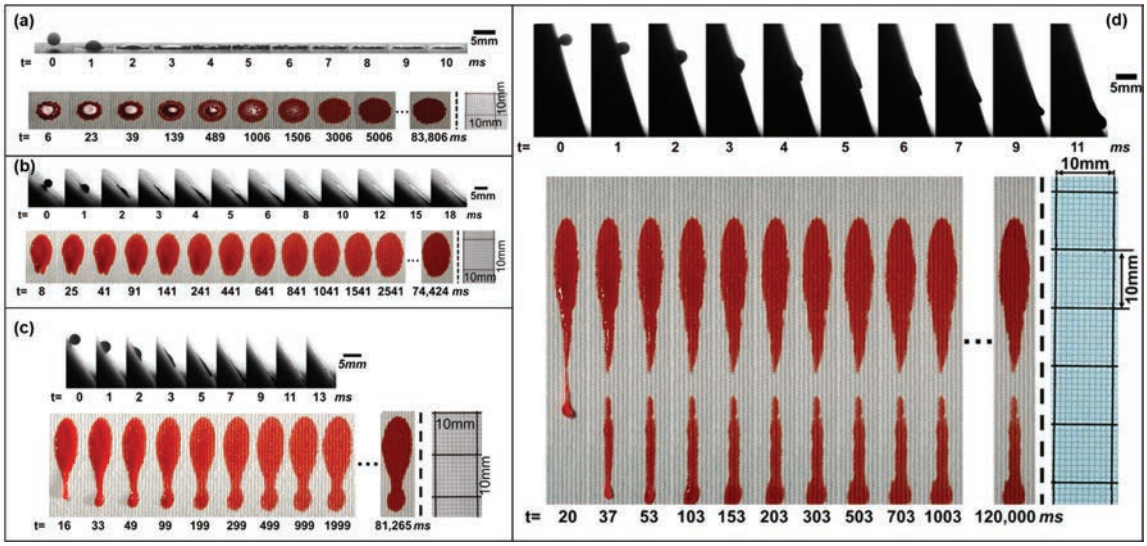

Figure 9. Sample results for blood drop inclined impact experiment. Blood droplet impact morphologies on the twill front surface at a fixed impact velocity with different impact angles including (a) 90°, (b) 45°, (c) 30°, and (d) 15°. In each box of images, the top denotes the side view from the high-speed video camera and the bottom denotes the inclined view from the DSLR camera.

Figures 9(b)-(d) demonstrate the case of inclined blood droplet impact and wicking process on the twill fabric surfaces. It is shown that with smaller drop impact angle *or* larger surface inclination), the tangential portion (along the slope of the inclined surface) of the impact velocity is higher, which significantly elongates the bloodstain shape along the inclined surface in the inertial impact and spreading

This resource was prepared by the author(s) using Federal funds provided by the U.S. Department of Justice. Opinions or points of view expressed are those of the author(s) and do not necessarily reflect the official position or policies of the U.S. Department of Justice.

process. Therefore, the resultant bloodstains found in the inclined impact scenario usually have larger aspect ratio than unity. In addition, the subsequent wicking process further enlarge the bloodstain area. It should be noted that the wicking-induced increase in the stain area occurs in both directions: along and perpendicular to the surface slope. Thus, it remains a question how the subsequent wicking process alters the bloodstain aspect ratio resulted from the inclined impact velocity? In the future, our planned quantitative, systematic analysis of the bloodstain images obtained from the "multiscale imaging setup" should provide an answer to this question, which however is not available at the completion of this project report. Last but not the least, in the experiment with different impact angles $15° \leq \alpha \leq 90°$), three typical resultant bloodstains were observed: "elliptical" shape (Fig. 9b), "bowling pin" shape (Fig. 9c), and "broken tail" shape (Fig. 9d).

4) Single micro blood drop generation and impact dynamics

As aforementioned, single micro-sized blood droplet interaction with textile surfaces was not resolved successfully in this project due to the technical difficulties in the visualization of the micro blood drop on the complex, structured fabric surfaces. Therefore, in this subsection, the reported results will just include the single micro blood drop generation and micro blood drop impact dynamics on non-textile surfaces.

The principle of the micro blood drop generation is based on the piezoelectric droplet-on-demand technology, which has been described in the method sections. A capillary nozzle is squeezed by a piezoelectric material actuated by high-voltage pulse. In this project, the influence of the pulse width on micro blood drop generation has been studied in detail. Figures 10(a)-(d) demonstrate the dynamics process describing the formation of micro blood droplets with four different pulse widths: $45\mu s$, $60\mu s$, $115\mu s$, and $140\mu s$. It is shown that there is an optimal range of pulse widths that will result in a perfect generation of single micro blood droplet. Outside this optimal range, there would be multiple blood droplets (Fig. 10a) generated at a time or no blood droplet ejection (Fig. 10d). A complete regime map regarding the influence of the pulse widths on micro blood drop generation can be found in Ref. [13].

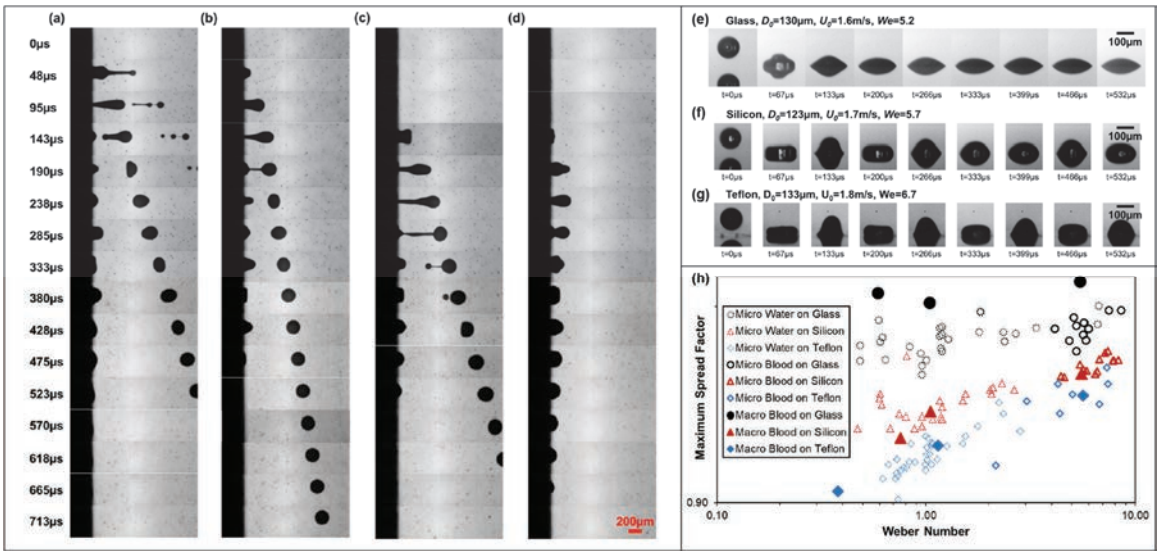

Figure 10. Sample results obtained in micro blood drop experiment. (a)-(d) Image sequences showing the micro blood droplet generation process with different pulse widths, including $45\mu s$, $60\mu s$, $115\mu s$, and $140\mu s$. (e)-(g) Image sequences showing the dynamics process after a micro blood droplet impacts onto the glass, silicon, and Teflon surfaces. (h) Comparison of the maximum spread factor for micro water droplets, micro blood droplets, and millimeter-sized blood droplets impacting on the glass, silicon, and Teflon surfaces.

Figures 10(e)-(g) demonstrate the image sequences showing the droplet impact process for micro blood droplet impacting onto glass, silicon, and Teflon surfaces. Teflon surface is the most hydrophobic surface and glass surface is the most hydrophilic one among the three tested surfaces. It is shown that on the surfaces with higher wettability (smaller contact angle), the spreading diameter of the impacting micro blood drop is larger. To investigate more about the micro blood drop impact dynamics, additional experiments with micro water droplets and macro-sized blood droplets were conducted. The maximum spread factors β_m) for these different experimental conditions were plotted together in Fig. 10(h). It is shown that on the silicon and Teflon surfaces, the maximum spread factor data for the micro water droplet, micro blood droplet, and millimeter-sized blood droplet roughly collapse into the same trend. Big deviation is observed for the Glass surface, on which the maximum spread factor from millimeter-sized droplet impact is higher than that from micro droplet impact.

5) Bloodstains formed on fabrics

In addition to digging into the blood drop impact and wicking dynamics, another important task in this project is to conduct the bloodstain pattern analysis for the bloodstains generated from single blood drop impacting onto those fabric surfaces. By utilizing the "multi-scale imaging system" and the "Inverse Perspective Mapping technique", a comprehensive bloodstain analysis in terms of both bloodstain area and bloodstain shape at any time instance after the blood droplet hits the textile surface becomes available. Upon the completion of this report, such bloodstain analysis has been carried out for blood droplets impacting on plain woven fabrics at different impact velocities.

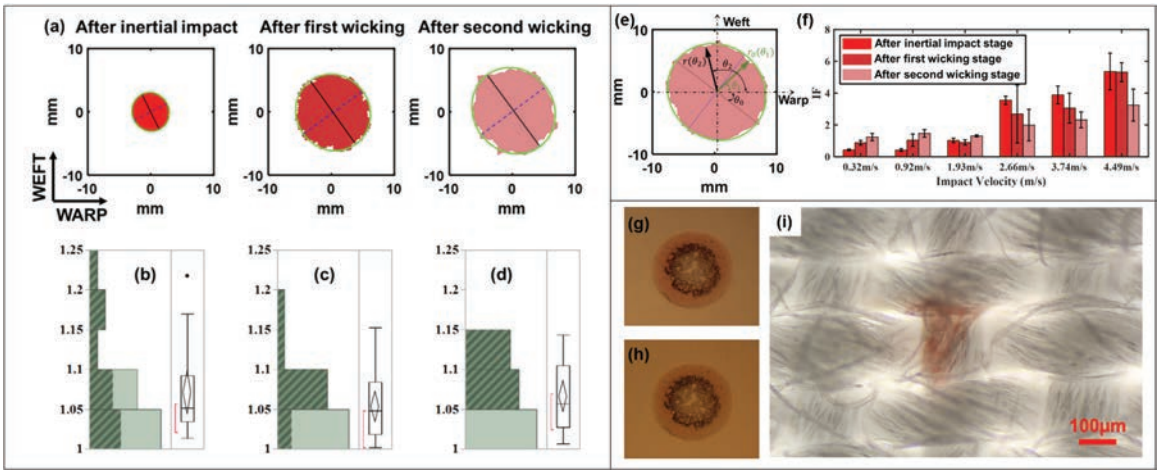

Figure 11. Analysis of bloodstains formed on textile surfaces. (a) Bloodstains at three distinct stages, and the distribution of the aspect ratio of the corresponding bloodstains after (b) the inertial impact stage, (c) the first-wicking stage, and (d) the second wicking stage. (e) Definition of the geometric parameters r, r_0, and θ for a bloodstain shape based on the fitted ellipse. (f) Comparison of the proposed irregularity factors at three different stages for blood droplet impacting onto the plain woven fabrics with different impact velocities. (g) Micro bloodstain on glass surface right after the micro blood droplet impact. (h Micro bloodstain on glass surface at 24 hours after the impact. (i) Micro bloodstain on the plain woven fabric surface.

The temporal evolution of the bloodstain area at different stages has been demonstrated in previous subsections when discussing the blood droplet impact and wicking dynamics. In this subsection, analysis of the bloodstain shape at corresponding stages is reported. To do the shape analysis for these bloodstains, a best-fit ellipse was obtained for each specific bloodstain. Figure 11(a) demonstrates sample reconstructed bloodstains by the IPM technique during the three distinct stages: after inertial impact, after the first-stage wicking process, and after the second-stage wicking process. Although in the case of perpendicular impact,

the resultant bloodstain on the plain woven fabric still tends to be an elliptical shape with an aspect ratio larger than one. Figures 11(b)-(d) summarize the distribution of the aspect ratios of those fitted ellipses to the bloodstains at the three stages. It is shown from Fig. 11(b) that the bloodstain aspect ratio can be as high as 1.25 right after the inertial impact process. It is observed from Figs. 11(c) and 11(d) that the subsequent wicking process generally narrows the aspect ratio distribution to the unity.

Besides the aspect ratio, another important aspect regarding the shape of bloodstains formed on textiles lies in the irregularity. It has been demonstrated by many previous works that the bloodstains on fabrics are distorted and irregular, which can hinder the correct interpretation of those bloodstains. In this project, we tried to quantify such irregularity of the bloodstains on fabrics by defining the following parameter called *irregularity factor* (*IF* :

$$IF = \sqrt{\sum_{2\pi}\left(\frac{r(\theta)-r_0(\theta)}{r_0(\theta)}\right)^2}. \quad (3$$

The definitions of $r(\theta)$ and $r_0(\theta)$ are illustrated in Fig. 11(e). In the schematic, θ_0 is the orientation angle of the bloodstain, with respect to the warp direction. $r_0(\theta)$ is the radius of the fitted ellipse at the angle of θ; and $r(\theta)$ is the radius of the real bloodstain at the angle of θ. Figure 11(f) further plots the values of the irregularity factor for different impact velocities. It is shown that IF increases with the increase in the impact velocity for all the three stages. The dependence of IF on the impact velocity becomes weaker after the wicking process. However, the dependence of IF on the impact velocity is still detectable and more obvious than the dependence of the final stain area or final bloodstain factor $\beta_{f,e}$) on the impact velocity, as compared to Figs. 7(c) and 8(g). This may suggest the possibility of utilizing the irregularity factor IF to estimate the impact velocity, which is important in BPA for crime scene reconstruction.

Finally, the micro bloodstains formed by the impact of single micro blood droplet are briefly reported in this subsection. Currently, only the micro bloodstains formed on the glass surface and plain woven have been investigated under an optical microscope as shown in Figs. 11(g)-(i). For micro bloodstains on glass surface, no difference was found between the bloodstains right after impact (Fig. 11g) and after 24 hours

(Fig. 11h). The volume of the micro blood droplet is only around 1.2nL and therefore the evaporation may finish as soon as the impacting micro blood drop reaches equilibrium spread on the surfaces. Another interesting finding regarding the micro bloodstains is that it presents certain zonal characteristics, which are similar to those observed for macro bloodstains [14]. Finally, for the micro bloodstain on the plain woven fabric surface, the micro bloodstain typically lands on the top of a single yarn of the fabric as shown in Fig. 11(i). The volume of the micro blood droplet is too tiny to saturate the yarn segment under the impacting droplet.

LIMITATIONS

The current imaging setup at the completion of this project was not capable of visualizing single micro blood droplet impacting and wicking process on the textile surfaces. This is because that for visualizing micro blood droplet, an extremely high shutter speed is required, which significantly reduces the amount of light going through the lens to form a bright image. Moreover, because the fabric surfaces are usually rough with complex surface structures, the lighting conditions at the textile surface are typically "diffusive reflection" rather than "specular reflection", which makes it hard to visualize the droplet spreading front. Another important reason for failing to visualize the micro blood droplet on textile surface is because of the complex structure of the fabrics. Usually at the surface top of a piece of fabric, there exists numerous random fibers standing on the surface top, which also hinders the view of the micro blood drop movement on the fabric surfaces.

ARTIFACTS

LIST OF PRODUCTS

1) Wang, F., Gallardo, V., Michielsen, S., & Fang, T. (2021). Fundamental study of porcine drip bloodstains on fabrics: Blood droplet impact and wicking dynamics. *Forensic Science International*, 318, 110614. **Journal Publication**

This resource was prepared by the author(s) using Federal funds provided by the U.S. Department of Justice. Opinions or points of view expressed are those of the author(s) and do not necessarily reflect the official position or policies of the U.S. Department of Justice.

2) Wang, F., Gallardo, V., Michielsen, S., & Fang, T. (2019, November). Drop-on-drop Impacts of Complex Liquids: the case of blood. *In APS Division of Fluid Dynamics Meeting Abstracts* pp. G21-007). (**Conference Presentation**

3) Wang, F., Gallardo, V., Michielsen, S., & Fang, T. (2019, November). Poster: Controlling desiccation pattern through droplet impacting. Conference: *72nd Annual Meeting of the APS Division of Fluid Dynamics*. (**Conference Poster**

4) Wang, F., Gallardo, V., Michielsen, S., & Fang, T., Effects of Surface Inclination on Blood Droplet Impacts on Twill Fabrics (**In preparation for *Forensic Science International***

5) Gallardo, V., Wang, F., Fang, T., & Michielsen, S., The Effect of Surface Roughness on Bloodstain Analysis (**In preparation for *Forensic Science International***

DATA SETS GENERATED

Based on the multiscale imaging and measurement system constructed in this project, the generated original dataset consists of the following:

high-speed videos showing instantaneous droplet impact process from the side view, high-speed videos showing the dynamic process from the tilted view 45º), and low-speed but high definition 720p) videos showing long-time wicking process were obtained **a)** for blood droplets impacting onto plain-woven fabrics at six different velocities, **b)** for blood droplets impacting onto five different fabric surfaces at three different velocities, and **c)** for blood droplets impacting onto the front of twill fabric at one fixed impact velocity with six different impact angles. Accordingly, macroscopic and microscopic bloodstain images (1× and 20×) right after impact and after 24 hours were also obtained for all the tested impact conditions.

DISSEMINATION ACTIVITIES

The first paper https://doi.org/10.1016/j.forsciint.2020.110614) based on this project has been published in the *Forensic Science International* journal, which focused on the fundamental droplet impact

dynamics and wicking dynamics during the formation of bloodstains resulted from millimeter-sized droplets impacts with different velocities. *Forensic Science International* is the flagship journal in the Forensic Science field, publishing the most innovative and influential contributions across the forensic sciences. Our paper published in this well-known forensic science journal enables a timely dissemination of the latest findings regarding bloodstain formation physics to the appropriate readers in the relevant field. We have also presented our work regarding (1) multiple blood droplets impacting dynamics and (2) bloodstain drying dynamics in the form of oral presentation and poster session respectively at the 72nd Annual Meeting of the American Physical Society Division of Fluid Dynamics in 2019. The presentation and poster session demonstrated the important fundamental fluid mechanics occurring in the bloodstain formation process in front of fluid mechanics experts around the world. Lastly, we are currently preparing two more manuscripts for publishing in forensic science journals, which will discuss the effects of surface inclination and the effects of textile surface roughness on the blood droplet impact dynamics and bloodstain interpretation.

References

1. Laber, T., Kish, P., Taylor, M., Owens, G., Osborne, N., & Curran, J. 2014). Reliability assessment of current methods in bloodstain pattern analysis. National Institute of Justice, US Department of Justice. https://www.ojp.gov/pdffiles1/nij/grants/247180.pdf
2. Michielsen S, Taylor M, Parekh N, Ji F 2015) Bloodstain Patterns on Textile Surfaces: A Fundamental Analysis. National Institute of Justice; Award No.: 2012-DN-BX-K052; https://www.ncjrs.gov/pdffiles1/nij/grants/248671.pdf
3. Chang, J. Y. M., & Michielsen, S. 2016). Effect of fabric mounting method and backing material on bloodstain patterns of drip stains on textiles. International journal of legal medicine, 130(3), 649-659.

4. Williams, E. M., Dodds, M., Taylor, M. C., Li, J., & Michielsen, S. (2016). Impact dynamics of porcine drip bloodstains on fabrics. Forensic science international, 262, 66-72.
5. Wang, F., Gallardo, V., Michielsen, S., & Fang, T. (2021). Fundamental study of porcine drip bloodstains on fabrics: Blood droplet impact and wicking dynamics. Forensic Science International, 318, 110614.
6. A. Monograph, "M7. Standard laboratory practice for home laundering fabrics prior to flammability testing to differentiate between durable and non-durable finishes." 2011.
7. "ASTM D1059-17, Standard Test Method for Yarn Number Based on Short-Length Specimens, ASTM International, West Conshohocken, PA, 2017, www.astm.org."
8. P. Agrawal, L. Barnet, and D. Attinger, "Bloodstains on woven fabric: Simulations and experiments for quantifying the uncertainty on the impact and directional angles," Forensic Sci. Int., vol. 278, pp. 240–252, 2017.
9. J. Li, X. Li, and S. Michielsen, "Alternative method for determining the original drop volume of bloodstains on knit fabrics," Forensic Sci. Int., vol. 263, pp. 194–203, 2016.
10. E. W. Washburn, "The dynamics of capillary flow," Phys. Rev., vol. 17, no. 3, p. 273, 1921.
11. E. Kissa, "Wetting and Wicking," Text. Res. J., vol. 66, no. 10, pp. 660–668, 1996.
12. T. Kawase, S. Sekoguchi, T. Fuj, and M. Minagawa, "Spreading of liquids in textile assemblies: Part I: Capillary spreading of liquids," Text. Res. J., vol. 56, no. 7, pp. 409–414, 1986.
13. Wang, F. (2020). Impact and Wicking Dynamics of Blood Droplets on Textile Surfaces. North Carolina State University. ProQuest Dissertations Publishing, 2020. 28276171.
14. D. Brutin, B. Sobac, B. Loquet, and J. Sampol, "Pattern formation in drying drops of blood," J. Fluid Mech., vol. 667, p. 85, 2011.